

# Quantum Magnetometer with Dual-Coupling Optomechanics

Gui-Lei Zhu,<sup>1</sup> Jing Liu,<sup>1,2</sup> Ying Wu,<sup>1</sup> and Xin-You Lü<sup>1,\*</sup>

<sup>1</sup>*School of Physics, Huazhong University of Science and Technology, Wuhan 430074, China*

<sup>2</sup>*MOE Key Laboratory of Fundamental Physical Quantities Measurement and PGMF, Huazhong University of Science and Technology, Wuhan 430074, China*

(Dated: May 3, 2022)

We propose an experimentally feasible magnetometer based on a dual-coupling optomechanical system, where the radiation-pressure coupling transduces the magnetic signal to the optical phase, and the quadratic optomechanical interaction induces a periodic squeezing effect. The latter not only amplifies the signal to be measured, but also accelerates the signal transducing rate characterized by an experimentally observable phase accumulation efficiency. In the vicinity of opto-mechanical decoupled time, the ultimate bound to the estimability of magnetic signal is proportional to  $\exp(-6r)$ , and then the optimized accuracy of estimation can be enhanced nearly 3 orders with a controllable squeezing parameter  $r < 1$ . Moreover, our proposal is robust against the mechanical thermal noise, and the sensitivity of a specific measurement can reach to the order of  $10^{-17}\text{T}/\sqrt{\text{Hz}}$  in the presence of dissipations and without ground state cooling of mechanical oscillator. Our proposal fundamentally broadens the fields of quantum metrology and cavity optomechanics, with potential application for on-chip magnetic detection with high precision.

Ultrasensitive magnetic detection has contributed immensely to a wide range of scientific areas from fundamental physics to advanced technologies, such as geological exploration, aerospace [1], biomedical imaging and diagnostics [2–4]. Over the past few decades, various magnetometers have been developed, including the superconducting quantum interference devices (SQUID) based on superconducting effects [5–7], spin-exchange relaxation-free atomic magnetometers [8–11], NV center magnetometers [12, 13] and Hall-effect sensors [14]. Normally, they require the elaborated operating conditions, such as the associated denoising technology and/or the complex signal read-out schemes [15], which reduces their capability of on-chip integration.

Cavity optomechanical system (OMS) [16–19] offers an alternative platform for the precision measurements of mass [20–22], weak forces [23–27], and magnetic fields [28–33]. Particularly, optomechanical magnetometer with high sensitivity has excellent quality of on-chip integration [34]. Recently, the YIG sphere-based optomechanical magnetometer has been experimentally demonstrated in Ref. [35], which have attained extremely low sensitivity values. In such magnetometers, the existence of Joule and Villari effects of magnetostrictive transducer [36], allows one to directly extract magnetic information by reading out the optical frequency shift (or transmission spectrum). Moreover, quantum metrology [37–40] points out that the quantum squeezing or entanglement [41–48] could improve the accuracy of parameter estimation in physical systems from the shot-noise limit to the Heisenberg limit, i.e., the optimal precision scales from  $1/\sqrt{N}$  to  $1/N$  with  $N$  being the number of resources employed in the measurements. This has stimulated enormous interests in exploiting quantum resources in the atoms (or spins) [49–52] and optical systems [53–56] for high-precision physical quantity measurements.

By applying quantum metrology to the detection of a static magnetic field, here we propose a quantum magnetometer based on a dual-coupling OMS, which has a periodic decoupling behavior between the optical and mechanical modes. The OMS supports two optical modes coupled simultaneously to the same mechanical mode, with radiation-pressure and quadratic optomechanical interactions, respectively [57–60]. The radiation-pressure coupling acts as a signal transducer, encoding the magnetic signal received by the mechanical oscillator into the optical phase. The quadratic optomechanical interaction amplifies both the signal to be measured and the signal transducing rate via inducing a periodic squeezing effect on the mechanical oscillator, whose maximum squeezing strength is determined by a controllable squeezing parameter  $r$ . By performing a homodyne detection on the optical phase within a wide time window around the first decoupled time  $\tau_1$ , the magnetic signal could be estimated with high precision.

To qualitatively characterize the precision of magnetometer, we define a displaced phase accumulation efficiency (PAE) that is experimentally observable via state tomography technique. By presenting the *exponentially* increased quantum Fisher information (QFI), i.e.,  $\mathcal{F}_q(\tau_1) \propto e^{12r}$ , we quantitatively demonstrate that the fundamental bound of measurement precision can be dramatically reduced even with a small squeezing parameter  $r$ . The periodic opto-mechanical decoupling makes the classical Fisher information (CFI) robust against the mechanical environment at the decoupled time, which in turn allows the sensitivity of a specific measurement to saturate the fundamental bound and reach to the order of  $10^{-17}\text{T}/\sqrt{\text{Hz}}$  in the presence of system dissipations. Moreover, the sensitivity to the order of  $\sim 10^{-15}\text{T}/\sqrt{\text{Hz}}$  is predicted even in the case of the thermal phonon number  $\bar{n}_{\text{th}} \sim 10^3$ . Our work establishes a connection

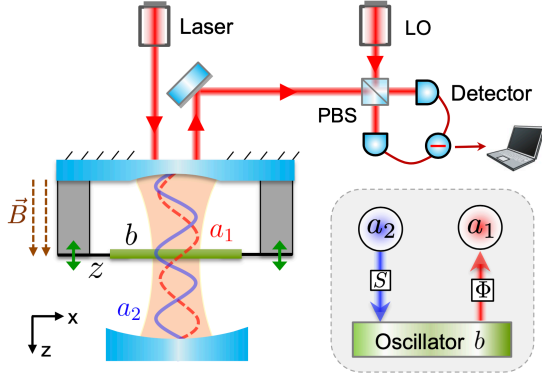


FIG. 1: Schematic illustration of quantum magnetometer based on a dual-coupling OMS with “membrane-in-the-middle” configuration. The middle SiN membrane (green), acting as the mechanical mode  $b$ , is welded to the ends of magnetostrictive Terfenol-D rods (gray) [61]. On application of a static magnetic field, the Terfenol-D rods expands, which displaces the equilibrium position of the mechanical mode, and then the magnetic signal is encoded into the phase  $\Phi$  of optical mode  $a_1$  via radiation-pressure coupling. Besides, cavity mode  $a_2$  offers the periodic squeezing for mode  $b$  via the quadratic optomechanical interaction [see the shaded area]. The optical phase is detected by the balanced homodyne detection scheme with a local oscillator (LO) pulse.

between quantum metrology and dual-coupling optomechanics, which is suitable for detecting various fields that linearly interact with the mechanical oscillator.

*System and periodic mechanical squeezing.*— We consider a dual-coupling optomechanical system depicted in Fig. 1 with Hamiltonian

$$H = \hbar\omega_1 a_1^\dagger a_1 + \hbar\omega_2 a_2^\dagger a_2 + \hbar\omega_m b^\dagger b - \hbar\lambda_1 a_1^\dagger a_1 (b^\dagger + b) - \hbar\lambda_2 a_2^\dagger a_2 (b^\dagger + b)^2 + B_z c_{\text{act}} z, \quad (1)$$

where  $a_j$  ( $j = 1, 2$ ) and  $b$  are the annihilation operators of the cavity mode with frequency  $\omega_j$  and the mechanical mode with frequency  $\omega_m$ , respectively. The mechanical membrane is placed at a node (antinode) of cavity mode  $a_1$  ( $a_2$ ), and then the fourth (fifth) term in Eq. (1) describes the radiation-pressure (quadratic optomechanical) interaction between modes  $a_1$  ( $a_2$ ) and  $b$  with strength  $\lambda_1$  ( $\lambda_2$ ). In the presence of a static magnetic field  $B_z$  (along  $z$  direction), the field-sensitive Terfenol-D expands, which leads to the change of the equilibrium position of the mechanical oscillator, thus generating an effective magnetic potential on the Hamiltonian, i.e., the last term of Equation (1) [62]. The mechanical motion modulates the optical cavity field via the nonlinear radiation-pressure coupling. Meanwhile, the phase shift of the mechanical motions encoded with magnetic signal is transferred to the optical field. By reading out the phase shift of optical field via homodyne detection, we can extract the original magnetic information. Here  $z = \sqrt{\hbar/(2m\omega_m)}(b^\dagger + b)$  is the position

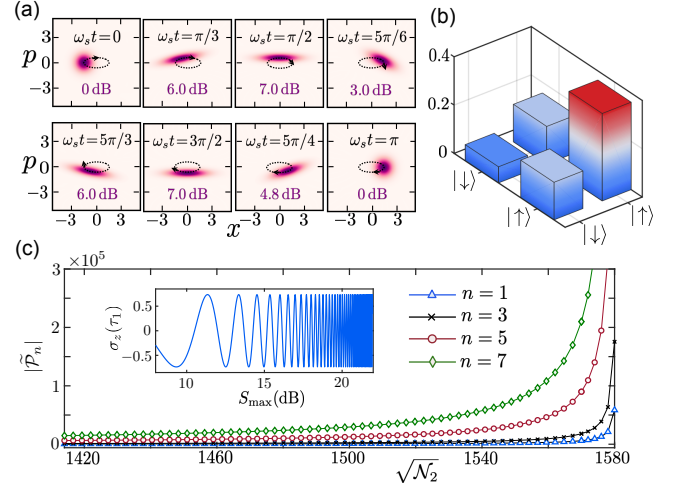


FIG. 2: (a) Wigner functions of the mechanical mode within  $2T$  given by  $a_1$  in vacuum state  $|0\rangle$ ,  $\omega_m = 1$  and  $\sqrt{\mathcal{N}_2} = 1414$ . The instantaneous squeezing degrees are marked. (b) Tomography of the state  $|\Psi(\tau_1)\rangle$  projected on the subspace  $\{| \downarrow \rangle, | \uparrow \rangle\}$  with  $l = 3$  and  $\sqrt{\mathcal{N}_2} = 1500$ . The dependence of  $\sigma_z(\tau_1)$  on the maximum squeezing degree  $S_{\text{max}}$  for  $l = 1$  and  $f = \omega_m$  is shown in the insert of (c). The main panel of (c) shows the absolute value of displaced PAE  $|\tilde{\mathcal{P}}_n|$  as a function of  $\sqrt{\mathcal{N}_2}$  for several values of  $n$ . The parameters are  $\omega_m = 2\pi \times 134$  kHz,  $f = 0.01\omega_m$ ,  $\alpha = 1$ ,  $\lambda_1 = 0.01\omega_m$ , and  $\lambda_2 = 10^{-7}\omega_m$ .

operator of the mechanical oscillator with mass  $m$ , and  $c_{\text{act}} = m\omega_m^2 L \alpha_{\text{mag}} / E$  is the magnetic actuation constant charactering how well the magnetic field is converted into a force applied on the oscillator. The symbol  $L$  denotes the length of Terfenol-D rods,  $\alpha_{\text{mag}}$  is magnetostrictive coefficient and  $E$  is the Young’s modulus [62].

By considering the ancillary mode  $a_2$  in the coherent state  $|\xi\rangle$ , the number operator  $a_2^\dagger a_2$  can be approximately replaced by an algebraic number  $\mathcal{N}_2 = |\xi|^2$  in the case of  $\mathcal{N}_2 \gg 1$  [62]. Assuming the modes  $a_1$  and  $b$  are initially in the coherent state  $|\Psi(0)\rangle = |\alpha\rangle \otimes |\beta\rangle$  with  $\beta = \beta_{\text{Re}} + i\beta_{\text{Im}}$ , the instantaneous state of system is given by [62]

$$|\Psi(t)\rangle = e^{-|\alpha|^2/2} \sum_{n=0}^{\infty} \frac{\alpha^n}{\sqrt{n!}} \exp[i\eta^2(\omega_s t - \sin \omega_s t)] \times \exp\{i\eta[\beta_{\text{Re}} \sin \omega_s t e^{-r} - \beta_{\text{Im}}(\cos \omega_s t - 1)e^r]\} |n\rangle |\varphi_s(t)\rangle, \quad (2)$$

where  $\eta = \lambda_s n / \omega_s - f_s / \omega_s$  with  $\lambda_s = \lambda_1 e^r$ ,  $\omega_s = \omega_m e^{-2r}$ ,  $f_s = f e^r = B_z c_{\text{act}} \sqrt{1/(2m\hbar\omega_m)} e^r$ ,  $r = -(1/4) \ln(1 - 4\lambda_2 \mathcal{N}_2 / \omega_m)$ , and a rotating frame with  $\exp(-i\omega_1 a_1^\dagger a_1 / \omega_s)$  was adopted. The mechanical state reads  $|\varphi_s(t)\rangle = S^\dagger(r) S(r') |\varphi_n(t)\rangle$  with the defined squeezing operator  $S(r) = \exp[r(b^2 - b^{\dagger 2})/2]$  and the squeezing parameter  $r' = r e^{-2i\omega_s t}$ . Here  $|\varphi_n(t)\rangle = |e^{-i\omega_s t} \beta + \eta \bar{\mu}\rangle$  is a displaced coherent state with  $\bar{\mu} = (1 - e^{-i\omega_s t})(\cosh r - e^{-i\omega_s t} \sinh r)$ . The expression of  $|\varphi_s(t)\rangle$  clearly shows that the mechanical mode is dy-

namically squeezed with the period  $T = \pi/\omega_s$ , whose squeezing degree of quadrature  $X = 1/\sqrt{2}(b + b^\dagger)$  is defined by  $S(t) = 10 \log_{10}(\delta X^2(t)/\delta X_{\min}^2)$  dB. The maximum squeezing degree  $S_{\max} = 10 \log_{10}(e^{4r})$  dB occurs at  $T/2$  with the state  $S^\dagger(2r)|\beta\rangle$  [62]. This periodic squeezing effect on the mechanical oscillator is induced by the quadratic optomechanical coupling, and can be qualitatively presented in the case of  $\alpha = \eta = 0$  [see Fig. 2(a)].

*Periodic-squeezing-enhanced phase accumulation efficiency.*— As shown in Eq. (2), the magnetic signal is transduced into the optical phase during the evolution of system via the radiation-pressure interaction. Interestingly, at time  $\tau_m = 2m\pi/\omega_s$  ( $m = 1, 2, \dots$ ), Eq. (2) can be reduced to [62]

$$|\Psi(\tau_m)\rangle = e^{-|\alpha|^2/2} \sum_{n=0}^{\infty} \frac{\alpha^n}{\sqrt{n!}} e^{i\Phi_n(\tau_m)} |n\rangle |\beta\rangle, \quad (3)$$

which demonstrates that the optical and mechanical modes are periodically decoupled, meanwhile the magnetic signal to be measured is periodically encoded into the accumulated optical phase  $\Phi_n(\tau_m) = 2m\pi(\lambda_s n/\omega_s - f_s/\omega_s)^2$  for a Fock state  $|n\rangle$ . Here the opto-mechanical decoupled period is double of the period of dynamical squeezing, i.e.,  $\tau_1 = 2\pi/\omega_s = 2T$ , and hence the mechanical squeezing also disappears at the decoupled time  $\tau_m$ .

The above unique property allows us to estimate the magnetic field  $B_z$  by performing a homodyne detection [see Fig. 1] on the optical mode  $a_1$  at the first decoupled time  $\tau_1$ . To qualitatively describe the detection precision, here we define a displaced PAE

$$\tilde{\mathcal{P}}_n = \frac{\Phi_n(\tau_1) - \Phi_0(\tau_1)}{\tau_1} = \frac{\lambda_1 n}{\omega_m} (\lambda_1 n - 2f) e^{4r}. \quad (4)$$

Obviously, the larger  $\tilde{\mathcal{P}}_n$ , i.e., the faster phase accumulation rate on the optical Fock state  $|n\rangle$ , the higher measurement accuracy of magnetometer should be obtained. As shown in Fig. 2(c), the  $\tilde{\mathcal{P}}_n$  is exponentially enhanced by increasing the coherent amplitude  $\sqrt{N_2}$  of the ancillary mode  $a_2$ . This enhancement originally comes from the periodic squeezing of mechanical mode during one opto-mechanical decoupled period [see Fig. 2(a)]. The system Hamiltonian in the squeezed frame shown in Eq. (S17) of supplementary material [62] clearly demonstrates that the mechanical squeezing effect not only accelerates the signal transducing rate from phonon to photon (i.e., the radiation-pressure interaction  $\lambda_s a_1^\dagger a_1 (b + b^\dagger)$ ) [63, 64], but also amplifies the magnetic signal to be measured (i.e., the magnetic potential  $f_s(b^\dagger + b)$ ).

More importantly, this well-defined PAE is experimentally observable via state tomography in the proper basis vectors. Specifically, expanding the system state  $|\Psi(\tau_1)\rangle$  in the subspace  $\{|\downarrow\rangle, |\uparrow\rangle\}$  with basis vectors

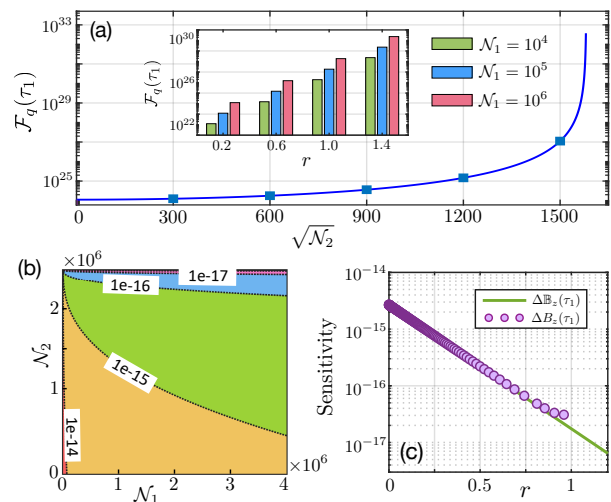


FIG. 3: (a) The QFI  $\mathcal{F}_q(\tau_1)$  versus  $\sqrt{N_2}$  (main) and  $r$  (inset). (b) Contour plot of the optimal sensitivity  $\Delta B_z(\tau_1)$  in units of T/ $\sqrt{\text{Hz}}$  as functions of  $N_1$  and  $N_2$ . (c)  $\Delta B_z(\tau_1)$  (solid curve) and the specific sensitivity  $\Delta B_z(\tau_1)$  in the presence of dissipations (circles) versus  $r$  for  $N_1 = 10^6$ . Here we have chosen  $m = 4 \times 10^{-8}$  g,  $L = 630$   $\mu\text{m}$ ,  $\alpha_{\text{mag}} = 5 \times 10^8$  NT $^{-1}$ m $^{-1}$ ,  $E = 30$  GPa,  $\kappa/\omega_m = 0.01$ ,  $\gamma/\omega_m = 0.001$ ,  $\bar{n}_{\text{th}} = 10$  and other parameters are same as Fig. 2.

$|\downarrow\rangle := (1/\sqrt{2})(|0\rangle - |l\rangle)$  and  $|\uparrow\rangle := (1/\sqrt{2})(|0\rangle + |l\rangle)$  ( $l = 1, 2, \dots$ ), we obtain four elements of density matrix [62], as shown in Fig. 2(b). The difference between two diagonal elements is denoted by  $\sigma_z(\tau_1) = \rho_{\uparrow\uparrow}(\tau_1) - \rho_{\downarrow\downarrow}(\tau_1) = 2e^{-|\alpha|^2} (\alpha^l/\sqrt{l!}) \cos(\Delta\Phi_l(\tau_1))$ , where  $\Delta\Phi_l(\tau_1) = \Phi_l(\tau_1) - \Phi_0(\tau_1)$ . Then one can easily obtain the values of phase difference  $\Delta\Phi_l(\tau_1)$  by directly measuring  $\rho_{\downarrow\downarrow}(\tau_1)$  and  $\rho_{\uparrow\uparrow}(\tau_1)$ , which ultimately leads to  $\tilde{\mathcal{P}}_l = \Delta\Phi_l(\tau_1)/\tau_1$  being experimentally observable. Moreover, the oscillation with increasing frequency of  $\sigma_z(\tau_1)$ , shown in the insert of Fig. 2(c), is another evidence for the enhanced  $\tilde{\mathcal{P}}_n$  along with increasing the mechanical squeezing.

*Quantum and classical Fisher information.*— From a quantitative point of view, the fundamental bound to the sensitivity and the measurement-specific sensitivity of the proposed magnetometer are respectively decided by the QFI  $\mathcal{F}_q$  and CFI  $\mathcal{F}_c$  based on the Cramér-Rao inequality  $\Delta B_z \geq 1/\sqrt{M\mathcal{F}_j}$  ( $j = q, c$ ), where  $\Delta B_z$  is the standard deviation with respect to an unbiased estimator  $(B_z)_{\text{est}}$ , and  $M$  is the number of repetition of the experiments [65].

Considering system state  $|\Psi(t)\rangle$ , the QFI with respect to the parameter  $B_z$  reads  $\mathcal{F}_q(t) = 4(\langle \partial_{B_z} \Psi(t) | \partial_{B_z} \Psi(t) \rangle - |\langle \Psi(t) | \partial_{B_z} \Psi(t) \rangle|^2)$ , where  $\partial_{B_z} = \partial/\partial B_z$  [66–70]. At the

first decoupled time  $\tau_1$ , the QFI reduces to [62]

$$\begin{aligned}\mathcal{F}_q(\tau_1) &= \frac{32\pi^2 m \lambda_1^2 L^2 \alpha_{\text{mag}}^2}{\hbar \omega_m E^2} \mathcal{N}_1 e^{12r}, \\ &= \frac{32\pi^2 m \lambda_1^2 L^2 \alpha_{\text{mag}}^2}{\hbar \omega_m E^2} \frac{\mathcal{N}_1}{[1 - (4\lambda_2/\omega_m)\mathcal{N}_2]^3}.\end{aligned}\quad (5)$$

where  $\mathcal{N}_1 = |\alpha|^2$  is the mean photon number of cavity mode  $a_1$ . It can be seen that the QFI is exponentially enhanced with power of  $12r$ , and hence increasing a small value of  $r$  by changing  $\mathcal{N}_2$  can give rise to a large enhancement of the QFI. Figure 3(a) shows an enhancement with 7 orders of magnitude for the QFI, corresponding to a dramatic reduction of the optimal sensitivity  $\Delta\mathbb{B}_z(\tau_1) = 1/\sqrt{M\mathcal{F}_q(\tau_1)}$ . As shown in Fig. 3(b), the optimal sensitivity  $\Delta\mathbb{B}_z(\tau_1)$  can reach to the order of  $10^{-15} - 10^{-17}(\text{T}/\sqrt{\text{Hz}})$  for a wide parameter region in terms of the mean photon numbers  $\mathcal{N}_1$  and  $\mathcal{N}_2$ . Equation (5) also indicates that the resources  $\mathcal{N}_1$  and  $\mathcal{N}_2$  exert different influences on the ultimate lower bound of sensitivity [62]. We note that the QFI at  $\tau_1$  does not depend on the actual value of  $B_z$ .

Next, let us calculate the CFI related to a specific measurement on the quadrature  $X_\theta = (a_1 e^{-i\theta} + a_1^\dagger e^{i\theta})/\sqrt{2}$ , where  $\theta$  is the phase of local oscillator. At the first decoupled time  $\tau_1$ , the CFI is given by [62]

$$\mathcal{F}_c(\tau_1) = \frac{32\pi^2 m \lambda_1^2 L^2 \alpha_{\text{mag}}^2}{\hbar \omega_m E^2} e^{12r} (\alpha_{\text{Re}} \sin \theta - \alpha_{\text{Im}} \cos \theta)^2. \quad (6)$$

Evidently, it consists precisely with the QFI shown in Eq. (5) when  $\theta = \pi/2$  ( $\theta = 0$ ) and  $\alpha$  is a real (imaginary) number, which means that the momentum (position) measurement can saturate the optimal sensitivity in the absence of system dissipation.

In the practical situation, the dissipation caused by the system-bath coupling should be taken into account. Then the dynamics of system is dominated by the master equation

$$\dot{\rho} = -\frac{i}{\hbar} [H, \rho] + \kappa \mathcal{D}[a_1]\rho + \gamma(\bar{n}_{\text{th}} + 1)\mathcal{D}[b]\rho + \gamma\bar{n}_{\text{th}}\mathcal{D}[b^\dagger]\rho, \quad (7)$$

where  $\kappa(\gamma)$  is the cavity (mechanical) decay rate,  $\bar{n}_{\text{th}}$  is the thermal phonon number of the mechanical mode, and  $\mathcal{D}[o]\rho = o\rho o^\dagger - (o^\dagger o \rho + \rho o^\dagger o)/2$ . Here we have considered the cavity mode  $a_2$  being in the coherent state  $|\xi\rangle$  for Hamiltonian  $H$ . Performing a momentum homodyne measurement (i.e.,  $\theta = \pi/2$ ) on cavity  $a_1$ , in Fig. 3(c) and Fig. 4, we numerically demonstrate the influence of system dissipation on the sensitivity limit, i.e.,  $\Delta B_z(\tau_1) = 1/\sqrt{M\mathcal{F}_c(\tau_1)}$ , of magnetometer [71].

With the practical experimental parameters, Figure 3(c) shows that the specific sensitivity  $\Delta B_z(\tau_1)$  obtained in the presence of system decay and noise, still can fit well with the optimal one  $\Delta\mathbb{B}_z(\tau_1)$  from the QFI without system dissipation. This consistency is only broken weakly when one increases the squeezing parameter

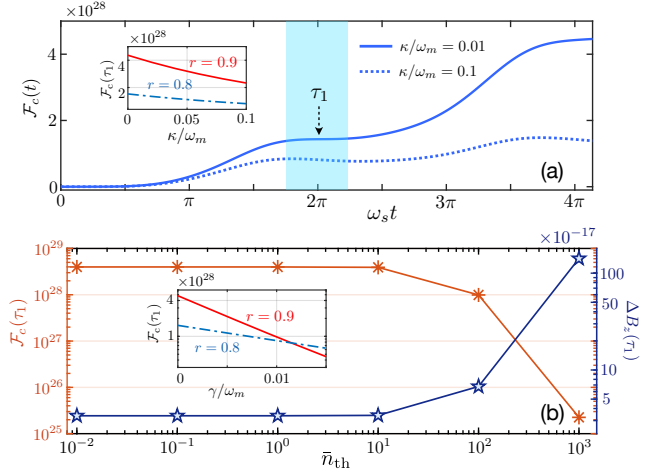


FIG. 4: (a) Time evolution of  $\mathcal{F}_c(t)$  for different values of  $\kappa/\omega_m$  in the presence of mechanical dissipation  $\gamma/\omega_m = 0.01$ ,  $\bar{n}_{\text{th}} = 10$  and considering  $r = 0.8$ . The shaded area indicates the time-window of detection with nearly flat  $\mathcal{F}_c(t)$  in the vicinity of the first decoupled time  $\tau_1$ . (b) CFI  $\mathcal{F}_c(\tau_1)$  (left y-axis) and specific sensitivity  $\Delta B_z(\tau_1)$  in units of  $\text{T}/\sqrt{\text{Hz}}$  (right y-axis) versus mechanical thermal phonon number  $\bar{n}_{\text{th}}$  for  $\kappa/\omega_m = 0.01$  and  $\gamma/\omega_m = 0.001$ . The insets show the influence of  $\kappa$  and  $\gamma$  on  $\mathcal{F}_c(\tau_1)$  for different values of squeezing parameter  $r$ .

$r$  to a large value. This can be explained as follows. On the one hand, system dissipation has little effect on the CFI  $\mathcal{F}_c(\tau_1)$  in the case of weak squeezing parameter  $r$  [see the inserts of Fig. 4]. More importantly, the periodic optomechanical decoupling makes the CFI robust against the mechanical thermal noise. As shown in Fig. 4(b), a high sensitivity reaching to the order of  $\sim 10^{-15} \text{T}/\sqrt{\text{Hz}}$  is allowed even when  $\bar{n}_{\text{th}} = 10^3$ . This means that the mechanical ground state cooling is not necessary for obtaining high-precision magnetometer in our proposal. On the other hand, the strong mechanical squeezing amplifies the effect of mechanical dissipation on CFI via effectively heating the environment (see the insert of Fig. 4(b) and Fig. S5 in supplementary material [62]), which leads to the weak disagreement between the measurement-specific sensitivity limit and the fundamental bound of sensitivity in the case of large values of  $r$ .

*Discussion of experimental feasibility.*— Regarding experimental implementations, while we have considered here a Febry-Pérot cavity with the membrane-in-the-middle configuration, our versatile proposal is not limited to this particular architecture. Based on the excellent controllability of the SQUID [72, 73], the transmission-line (TL) resonator coupled to a SQUID-terminated TL resonator is a promising platform to realize dual-coupling optomechanical system [74, 75]. Recently, the dual-coupling optomechanics was also demonstrated in photonic crystal cavities [76, 77] and whispering gallery

microcavities [78]. Based on recent optomechanical experiments [57, 58, 79], here the system parameters can be chosen as  $m = 4 \times 10^{-8}$  g,  $\omega_m = 2\pi \times 134$  kHz,  $\lambda_1 = 8.4$  kHz,  $\lambda_2 = 0.08$  Hz,  $\kappa = 8.4$  kHz,  $\gamma = 840$  Hz, and  $\mathcal{N}_1 = 10^6$ . Then, with a cycle time on tens of  $\mu$ s, our work theoretically predicts that the sensitivity in the range of  $10^{-15} - 10^{-17}$  T/ $\sqrt{\text{Hz}}$  can be realized with the achievable squeezing parameter  $r \in [0, 0.9]$ . Note that most of the above results are obtained in the case of performing the homodyne measurement at the first decoupled time  $\tau_1$ . Fortunately, our proposal is robust against the detection time, i.e., the CFI in the vicinity of  $\tau_1$  is nearly flat as shown in Figure 4(a). In other words, our proposal exhibits a wide time-window to perform measurement with sensitivity reaching to the order of  $10^{-17}$  T/ $\sqrt{\text{Hz}}$ .

Moreover, the experimental implementation of our proposal relies on the thin membrane held by Terfenol-D rods, which gives an effective magnetic potential on the Hamiltonian. The conversion efficiency from the applied magnetic field to an effective force on the mechanical oscillator, is determined by the magnetic actuation constant  $c_{\text{act}}$ . The precise experimental determination of the magnetic actuation constant is of key importance for measuring afterwards accurate values of the magnetic field. This magnetic constant depends heavily on the specific geometrical configuration of the rods with respect to the membrane. To optimize the magnetostrictive effect, the applied magnetic field needs to be paralleled to the magnetostrictive direction of the Terfenol-D rods. In addition, here we considered the Terfenol-D rods of the length  $\sim 10^{-5}$  m, thus it is approximatively valid to consider the magnetostrictive material to be in the whole homogeneous magnetic field, which also allows the system to have a large actuation constant.

Despite here we focus on detecting a static magnetic field, our proposal, in principle, can also be applied to probe the alternating magnetic fields. The corresponding frequency response characteristics are discussed in Sec. VII of the supplementary material [62]. Referring to the parameters used in optomechanical experiments [34, 57], we numerically simulate the displacement noise power spectrum and the corresponding force sensitivity at different probe powers (see Fig. S6 in the supplementary material). We find that the thermal-noise-limited frequency range covers  $0 \sim 380$  kHz with the central resonant frequency 250 kHz in the case of the probe power at 20 nW. Therefore, similar as a general optomechanical system [34], here the dual-coupling magnetometer also has a broad bandwidth, when it is used as a resonant sensor.

*Conclusions.*— We have presented a protocol to measure the weak magnetic field using dual-coupling optomechanics. The sensitivity could be enhanced to the order of  $10^{-15} - 10^{-17}$  T/ $\sqrt{\text{Hz}}$  by adjusting the photon numbers of two cavity modes. This enhancement originally

comes from the periodic mechanical squeezing, which greatly amplifies both the signal to be measured and the transducing rate of signal. We stress out that this periodic squeezing effect is self-sustained, which avoids the complicated process of preparing squeezed states. Our proposal, with wide time-window of detection, is robust against the mechanical thermal noise, and hence the ground state cooling of mechanical mode is not necessary. This work might inspire the studies of high-precision measurements of various physical quantities based on dual-coupling optomechanical systems.

*Acknowledgments.*— We thank Bei-Bei Li for fruitful discussions and valuable comments. This work is supported by the National Key Research and Development Program of China grant 2021YFA1400700 and the National Science Foundation of China (Grant Nos. 11822502, 11974125, 11875029, 12175075 and 11805073).

---

\* Electronic address: [xinyoulu@hust.edu.cn](mailto:xinyoulu@hust.edu.cn)

- [1] J. S. Bennett, B. E. Vyhnalek, H. Greenall, E. M. Bridge, F. Gotardo, S. Forstner, G. I. Harris, F. A. Miranda, and W. P. Bowen, Precision magnetometers for aerospace applications: A review, *Sensors* **21**, 5568 (2021).
- [2] M. Hämmäläinen, R. Hari, R. J. Ilmoniemi, J. Knuutila, and O. V. Lounasmaa, Magnetoencephalography-theory, instrumentation, and applications to noninvasive studies of the working human brain, *Rev. Mod. Phys.* **65**, 413 (1993).
- [3] H. Lee, T.-H. Shin, J. Cheon, and R. Weissleder, Recent developments in magnetic diagnostic systems, *Chem. Rev.* **115**, 10690 (2015).
- [4] D. Murzin, D. J. Mapps, K. Levada, V. Belyaev, A. Omelyanchik, L. Panina, and V. Rodionova, Ultrasensitive magnetic field sensors for biomedical applications, *Sensors* **20**, 1569 (2020).
- [5] R. C. Jaklevic, J. Lambe, A. H. Silver, and J. E. Mercereau, Quantum interference effects in josephson tunneling, *Phys. Rev. Lett.* **12**, 159 (1964).
- [6] S. N. Erné, H.-D. Hahlbohm, and H. Lübbig, Theory of rf-biased superconducting quantum interference device for nonhysteretic regime, *J. Appl. Phys.* **47**, 5440 (1976).
- [7] R. Kleiner, D. Koelle, F. Ludwig, and J. Clarke, Superconducting quantum interference devices: State of the art and applications, *Proceedings of the IEEE* **92**, 1534 (2004).
- [8] J. C. Allred, R. N. Lyman, T. W. Kornack, and M. V. Romalis, High-sensitivity atomic magnetometer unaffected by spin-exchange relaxation, *Phys. Rev. Lett.* **89**, 130801 (2002).
- [9] I. K. Kominis, T. W. Kornack, J. C. Allred, and M. V. Romalis, A subfemtotesla multichannel atomic magnetometer, *Nature* **422**, 596 (2003).
- [10] I. M. Savukov, S. J. Seltzer, M. V. Romalis, and K. L. Sauer, Tunable atomic magnetometer for detection of radio-frequency magnetic fields, *Phys. Rev. Lett.* **95**, 063004 (2005).
- [11] H. Xia, A. Ben-Amar Baranga, D. Hoffman, and M. V. Romalis, Magnetoencephalography with an atomic mag-

- netometer, *Appl. Phys. Lett.* **89**, 211104 (2006).
- [12] J. M. Taylor, P. Cappellaro, L. Childress, L. Jiang, D. Budker, P. R. Hemmer, A. Yacoby, R. Walsworth, and M. D. Lukin, High-sensitivity diamond magnetometer with nanoscale resolution, *Nat. Phys.* **4**, 810 (2008).
- [13] J. R. Maze, P. L. Stanwix, J. S. Hodges, S. Hong, J. M. Taylor, P. Cappellaro, L. Jiang, M. V. G. Dutt, E. Togan, A. S. Zibrov, A. Yacoby, R. L. Walsworth, and M. D. Lukin, Nanoscale magnetic sensing with an individual electronic spin in diamond, *Nature* **455**, 644 (2008).
- [14] S. J. Bending, Local magnetic probes of superconductors, *Advances in Physics* **48**, 449 (1999).
- [15] D. Robbes, Highly sensitive magnetometers—a review, *Sens. Actu. A: Phys.* **129**, 86 (2006).
- [16] M. Aspelmeyer, T. J. Kippenberg, and F. Marquardt, Cavity optomechanics, *Rev. Mod. Phys.* **86**, 1391 (2014).
- [17] T. J. Kippenberg and K. J. Vahala, Cavity optomechanics: Back-action at the mesoscale, *Science* **321**, 1172 (2008).
- [18] M. Aspelmeyer, P. Meystre, and K. Schwab, Quantum optomechanics, *Physics Today* **65**, 29 (2012).
- [19] P. Meystre, A short walk through quantum optomechanics, *Ann. Phys.* **525**, 215 (2013).
- [20] J.-J. Li and K.-D. Zhu, Nonlinear optical mass sensor with an optomechanical microresonator, *Appl. Phys. Lett.* **101**, 141905 (2012).
- [21] Q. Lin, B. He, and M. Xiao, Mass sensing by detecting the quadrature of a coupled light field, *Phys. Rev. A* **96**, 043812 (2017).
- [22] S.-W. Bin, X.-Y. Lü, T.-S. Yin, G.-L. Zhu, Q. Bin, and Y. Wu, Mass sensing by quantum criticality, *Opt. Lett.* **44**, 630 (2019).
- [23] A. A. Clerk, M. H. Devoret, S. M. Girvin, F. Marquardt, and R. J. Schoelkopf, Introduction to quantum noise, measurement, and amplification, *Rev. Mod. Phys.* **82**, 1155 (2010).
- [24] M. Tsang and C. M. Caves, Coherent quantum-noise cancellation for optomechanical sensors, *Phys. Rev. Lett.* **105**, 123601 (2010).
- [25] A. Pontin, M. Bonaldi, A. Borrielli, F. S. Cataliotti, F. Marino, G. A. Prodi, E. Serra, and F. Marin, Detection of weak stochastic forces in a parametrically stabilized micro-optomechanical system, *Phys. Rev. A* **89**, 023848 (2014).
- [26] F. Armata, L. Latmiral, A. D. K. Plato, and M. S. Kim, Quantum limits to gravity estimation with optomechanics, *Phys. Rev. A* **96**, 043824 (2017).
- [27] S. Qvarfort, A. Serafini, P. F. Barker, and S. Bose, Gravimetry through non-linear optomechanics, *Nat. Commun.* **9**, 3690 (2018).
- [28] S. Forstner, S. Prams, J. Knittel, E. D. van Ooijen, J. D. Swaim, G. I. Harris, A. Szorkovszky, W. P. Bowen, and H. Rubinsztein-Dunlop, Cavity optomechanical magnetometer, *Phys. Rev. Lett.* **108**, 120801 (2012).
- [29] S. Forstner, E. Sheridan, J. Knittel, C. L. Humphreys, G. A. Brawley, H. Rubinsztein-Dunlop, and W. P. Bowen, Ultrasensitive optomechanical magnetometry, *Adv. Mater.* **26**, 6348 (2014).
- [30] C. Yu, J. Janousek, E. Sheridan, D. L. McAuslan, H. Rubinsztein-Dunlop, P. K. Lam, Y. Zhang, and W. P. Bowen, Optomechanical magnetometry with a macroscopic resonator, *Phys. Rev. Appl.* **5**, 044007 (2016).
- [31] M. Wu, N. L.-Y. Wu, T. Firdous, F. Fani Sani, J. E. Losby, M. R. Freeman, and P. E. Barclay, Nanocavity optomechanical torque magnetometry and radiofrequency susceptometry, *Nat. Nanotech.* **12**, 127 (2017).
- [32] J. Zhu, G. Zhao, I. Savukov, and L. Yang, Polymer encapsulated microcavity optomechanical magnetometer, *Sci. Rep.* **7**, 8896 (2017).
- [33] B.-B. Li, J. Bilek, U. B. Hoff, L. S. Madsen, S. Forstner, V. Prakash, C. Schäfermeier, T. Gehring, W. P. Bowen, and U. L. Andersen, Quantum enhanced optomechanical magnetometry, *Optica* **5**, 850 (2018).
- [34] B.-B. Li, L. Ou, Y. Lei, and Y.-C. Liu, Cavity optomechanical sensing, *Nanophotonics* **10**, 2799 (2021).
- [35] M. F. Colombano, G. Arregui, F. Bonell, N. E. Capuj, E. Chavez-Angel, A. Pitanti, S. O. Valenzuela, C. M. Sotomayor-Torres, D. Navarro-Urrios, and M. V. Costache, Ferromagnetic resonance assisted optomechanical magnetometer, *Phys. Rev. Lett.* **125**, 147201 (2020).
- [36] A. Olabi and A. Grunwald, Design and application of magnetostrictive materials, *Materials & Design* **29**, 469 (2008).
- [37] V. Giovannetti, S. Lloyd, and L. Maccone, Quantum-enhanced measurements: Beating the standard quantum limit, *Science* **306**, 1330 (2004).
- [38] V. Giovannetti, S. Lloyd, and L. Maccone, Quantum metrology, *Phys. Rev. Lett.* **96**, 010401 (2006).
- [39] V. Giovannetti, S. Lloyd, and L. Maccone, Advances in quantum metrology, *Nat. Photon.* **5**, 222 (2011).
- [40] J. P. Dowling and K. P. Seshadreesan, Quantum optical technologies for metrology, sensing, and imaging, *J. Lightwave Technol.* **33**, 2359 (2015).
- [41] C. M. Caves, Quantum-mechanical noise in an interferometer, *Phys. Rev. D* **23**, 1693 (1981).
- [42] J. Ma, X. Wang, C. Sun, and F. Nori, Quantum spin squeezing, *Phys. Rep.* **509**, 89 (2011).
- [43] T. Baumgratz and A. Datta, Quantum enhanced estimation of a multidimensional field, *Phys. Rev. Lett.* **116**, 030801 (2016).
- [44] C. L. Degen, F. Reinhard, and P. Cappellaro, Quantum sensing, *Rev. Mod. Phys.* **89**, 035002 (2017).
- [45] N. J. Engelsen, R. Krishnakumar, O. Hosten, and M. A. Kasevich, Bell correlations in spin-squeezed states of 500 000 atoms, *Phys. Rev. Lett.* **118**, 140401 (2017).
- [46] T. Nagata, R. Okamoto, J. L. O'Brien, K. Sasaki, and S. Takeuchi, Beating the standard quantum limit with four-entangled photons, *Science* **316**, 726 (2007).
- [47] Y. Israel, S. Rosen, and Y. Silberberg, Supersensitive polarization microscopy using noon states of light, *Phys. Rev. Lett.* **112**, 103604 (2014).
- [48] X.-Y. Luo, Y.-Q. Zou, L.-N. Wu, Q. Liu, M.-F. Han, M. K. Tey, and L. You, Deterministic entanglement generation from driving through quantum phase transitions, *Science* **355**, 620 (2017).
- [49] J. A. Jones, S. D. Karlen, J. Fitzsimons, A. Ardavan, S. C. Benjamin, G. A. D. Briggs, and J. J. L. Morton, Magnetic field sensing beyond the standard quantum limit using 10-spin noon states, *Science* **324**, 1166 (2009).
- [50] T. Tanaka, P. Knott, Y. Matsuzaki, S. Dooley, H. Yamaguchi, W. J. Munro, and S. Saito, Proposed robust entanglement-based magnetic field sensor beyond the standard quantum limit, *Phys. Rev. Lett.* **115**, 170801 (2015).
- [51] P. Kómár, E. M. Kessler, M. Bishof, L. Jiang, A. S. Sørensen, J. Ye, and M. D. Lukin, A quantum network of clocks, *Nat. Phys.* **10**, 582 (2014).

- [52] Z. Hou, Z. Zhang, G.-Y. Xiang, C.-F. Li, G.-C. Guo, H. Chen, L. Liu, and H. Yuan, Minimal tradeoff and ultimate precision limit of multiparameter quantum magnetometry under the parallel scheme, *Phys. Rev. Lett.* **125**, 020501 (2020).
- [53] M. J. Holland and K. Burnett, Interferometric detection of optical phase shifts at the heisenberg limit, *Phys. Rev. Lett.* **71**, 1355 (1993).
- [54] A. N. Boto, P. Kok, D. S. Abrams, S. L. Braunstein, C. P. Williams, and J. P. Dowling, Quantum interferometric optical lithography: Exploiting entanglement to beat the diffraction limit, *Phys. Rev. Lett.* **85**, 2733 (2000).
- [55] P. M. Anisimov, G. M. Raterman, A. Chiruvelli, W. N. Plick, S. D. Huver, H. Lee, and J. P. Dowling, Quantum metrology with two-mode squeezed vacuum: Parity detection beats the heisenberg limit, *Phys. Rev. Lett.* **104**, 103602 (2010).
- [56] J. Joo, W. J. Munro, and T. P. Spiller, Quantum metrology with entangled coherent states, *Phys. Rev. Lett.* **107**, 083601 (2011).
- [57] J. D. Thompson, B. M. Zwickl, A. M. Jayich, F. Marquardt, S. M. Girvin, and J. G. E. Harris, Strong dispersive coupling of a high-finesse cavity to a micromechanical membrane, *Nature* **452**, 72 (2008).
- [58] J. C. Sankey, C. Yang, B. M. Zwickl, A. M. Jayich, and J. G. E. Harris, Strong and tunable nonlinear optomechanical coupling in a low-loss system, *Nat. Phys.* **6**, 707 (2010).
- [59] M. Bhattacharya, H. Uys, and P. Meystre, Optomechanical trapping and cooling of partially reflective mirrors, *Phys. Rev. A* **77**, 033819 (2008).
- [60] G.-L. Zhu, X.-Y. Lü, L.-L. Wan, T.-S. Yin, Q. Bin, and Y. Wu, Controllable nonlinearity in a dual-coupling optomechanical system under a weak-coupling regime, *Phys. Rev. A* **97**, 033830 (2018).
- [61] C. Hong, Application of a magnetostrictive actuator, *Materials and Design* **46**, 617 (2013).
- [62] See more information in Supplementary Material.
- [63] X.-Y. Lü, Y. Wu, J. R. Johansson, H. Jing, J. Zhang, and F. Nori, Squeezed optomechanics with phase-matched amplification and dissipation, *Phys. Rev. Lett.* **114**, 093602 (2015).
- [64] M.-A. Lemonde, N. Didier, and A. A. Clerk, Enhanced nonlinear interactions in quantum optomechanics via mechanical amplification, *Nat. Commun.* **7**, 11338 (2016).
- [65] S. L. Braunstein and C. M. Caves, Statistical distance and the geometry of quantum states, *Phys. Rev. Lett.* **72**, 3439 (1994).
- [66] M. G. A. Paris, Quantum estimation for quantum technology, *Int. J. Quantum Inf.* **07**, 125 (2009).
- [67] G. Tóth and I. Apellaniz, Quantum metrology from a quantum information science perspective, *J. Phys. A: Math. Theor.* **47**, 424006 (2014).
- [68] J. Liu, H. Yuan, X.-M. Lu, and X. Wang, Quantum fisher information matrix and multiparameter estimation, *J. Phys. A: Math. Theor.* **53**, 023001 (2019).
- [69] X.-M. Lu and X. Wang, Incorporating heisenberg's uncertainty principle into quantum multiparameter estimation, *Phys. Rev. Lett.* **126**, 120503 (2021).
- [70] J. Liu, M. Zhang, H. Chen, L. Wang, and H. Yuan, Optimal scheme for quantum metrology, *Advanced Quantum Technologies* **5**, 2100080 (2022).
- [71] J. Johansson, P. Nation, and F. Nori, Qutip: An open-source python framework for the dynamics of open quantum systems, *Comput. Phys. Commun.* **183**, 1760 (2012).
- [72] J. Q. You and F. Nori, Atomic physics and quantum optics using superconducting circuits, *Nature* **474**, 589 (2011).
- [73] Z.-L. Xiang, S. Ashhab, J. Q. You, and F. Nori, Hybrid quantum circuits: Superconducting circuits interacting with other quantum systems, *Rev. Mod. Phys.* **85**, 623 (2013).
- [74] J. R. Johansson, G. Johansson, and F. Nori, Optomechanical-like coupling between superconducting resonators, *Phys. Rev. A* **90**, 053833 (2014).
- [75] E.-j. Kim, J. R. Johansson, and F. Nori, Circuit analog of quadratic optomechanics, *Phys. Rev. A* **91**, 033835 (2015).
- [76] M. Kalaei, T. K. Paraiso, H. Pfeifer, and O. Painter, Design of a quasi-2d photonic crystal optomechanical cavity with tunable, large  $x^2$ -coupling, *Opt. Express* **24**, 21308 (2016).
- [77] M. Brunelli, O. Houhou, D. W. Moore, A. Nunnenkamp, M. Paternostro, and A. Ferraro, Unconditional preparation of nonclassical states via linear-and-quadratic optomechanics, *Phys. Rev. A* **98**, 063801 (2018).
- [78] H.-K. Li, Y.-C. Liu, X. Yi, C.-L. Zou, X.-X. Ren, and Y.-F. Xiao, Proposal for a near-field optomechanical system with enhanced linear and quadratic coupling, *Phys. Rev. A* **85**, 053832 (2012).
- [79] C. F. Ockeloen-Korppi, E. Damskägg, J.-M. Pirkkalainen, M. Asjad, A. A. Clerk, F. Massel, M. J. Woolley, and M. A. Sillanpää, Stabilized entanglement of massive mechanical oscillators, *Nature* **556**, 478 (2018).